

See discussions, stats, and author profiles for this publication at: <https://www.researchgate.net/publication/234513252>

Estimated velocities and inferred cause of overwash that emplaced inland fields of cobbles and boulders at Anegada, British Virgin Islands

Article · November 2010

CITATIONS

9

READS

52

4 authors, including:



Mark Lawrence Buckley

United States Geological Survey

45 PUBLICATIONS 681 CITATIONS

[SEE PROFILE](#)



Yong Wei

National Oceanic and Atmospheric Administration

79 PUBLICATIONS 1,319 CITATIONS

[SEE PROFILE](#)



Bruce E Jaffe

United States Geological Survey

191 PUBLICATIONS 5,541 CITATIONS

[SEE PROFILE](#)

Some of the authors of this publication are also working on these related projects:



Sea-level Rise Impacts on Low-latitude Carbonate Coasts [View project](#)



CASCaDE [View project](#)

Inverse modeling of velocities and inferred cause of overwash that emplaced inland fields of boulders at Anegada, British Virgin Islands

Mark L. Buckley · Yong Wei · Bruce E. Jaffe · Steve G. Watt

Received: 1 April 2010 / Accepted: 3 January 2011
© US Government 2011

Abstract A combination of numeric hydrodynamic models, a large-clast inverse sediment-transport model, and extensive field measurements were used to discriminate between a tsunami and a storm striking Anegada, BVI a few centuries ago. In total, 161 cobbles and boulders were measured ranging from 1.5 to 830 kg at distances of up to 1 km from the shoreline and 2 km from the crest of a fringing coral reef. Transported clasts are composed of low porosity limestone and were derived from outcrops in the low lying interior of Anegada. Estimates of the near-bed flow velocities required to transport the observed boulders were calculated using a simple sediment-transport model, which accounts for fluid drag, inertia, buoyancy, and lift forces on boulders and includes both sliding and overturning transport mechanisms. Estimated near-bed flow velocities are converted to depth-averaged velocities using a linear eddy viscosity model and compared with water level and depth-averaged velocity time series from high-resolution coastal inundation models. Coastal inundation models simulate overwash by the storm surge and waves of a category 5 hurricane and tsunamis from a Lisbon earthquake of M 9.0 and two hypothetical earthquakes along the North America Caribbean Plate boundary. A modeled category 5 hurricane and three simulated tsunamis were all capable of inundating the boulder fields and transporting a portion of the observed clasts, but **only an earthquake of M 8.0 on a normal fault of the outer rise along the Puerto Rico Trench was found to be capable of transporting the largest clasts at their current locations.** Model results show that

Electronic supplementary material The online version of this article (doi:[10.1007/s11069-011-9725-8](https://doi.org/10.1007/s11069-011-9725-8)) contains supplementary material, which is available to authorized users.

M. L. Buckley (✉) · B. E. Jaffe · S. G. Watt
Pacific Coastal and Marine Science Center, US Geological Survey, 400 Natural Bridges Drive,
Santa Cruz, CA 95060, USA
e-mail: mbuckley@usgs.gov

Y. Wei
Pacific Marine Environmental Laboratory (PMEL), National Oceanic and Atmospheric Administration
(NOAA), Joint Institute for the Study of the Atmosphere and Ocean (JISAO), University
of Washington, 7600 Sand Point Way NE, Seattle, WA 98115, USA

while both storm waves and tsunamis are capable of generating velocities and temporal acceleration necessary to transport large boulders near the reef crest, attenuation of wave energy due to wave breaking and bottom friction limits the capacity of storm waves to transport large clast at great inland distances. Through sensitivity analysis, we show that even when using coefficients in the sediment-transport model which yield the lowest estimated minimum velocities for boulder transport, storm waves from a category 5 hurricane are not capable of transporting the largest boulders in the interior of Anegada. Because of the uncertainties in the modeling approach, extensive sensitivity analyses are included and limitations are discussed.

Keywords Boulder · Tsunami · Hurricane · Cyclone · British Virgin Islands · Caribbean

1 Introduction

Boulders transported by extreme waves have the potential to provide a record of the occurrence and characteristics of past events. The utility of boulder deposits in assessing prehistoric tsunamis or storms is often limited by the lack of stratigraphic context, making correlation and dating of an event difficult (Dawson et al. 2008). In addition to the lack of stratigraphic context, boulders can be transported by both storm waves (Goto et al. 2009; Morton et al. 2008 and references therein; Hall et al. 2006) and tsunamis (Goto et al. 2007; Paris et al. 2009; Goff et al. 2006) requiring methods for distinguishing between the two types of events. Attempts have been made to calculate the minimum wave height required to transport boulders by either storm waves or tsunamis (Nott 2003; Noormets et al. 2004), but are controversial (Morton et al. 2006; Goto et al. 2009; Spiske et al. 2008) largely due to the simplifying assumptions used. Assumptions include the treatment of particle shape and porosity (see Spiske et al. 2008 for discussion), treatment of inertia force (see Morton et al. 2006 for discussion), transport mechanism (see Goto et al. 2009 for discussion), and methods of relating near-bed current velocity to tsunami and storm wave heights (see Goto et al. 2009 for discussion).

Because of the unique nature of the study site and the comprehensive approach taken here, we are able to avoid many of the controversial aspects of past extreme-wave boulder deposit studies listed above. A portion of the boulders is deposited within a sheet of sand allowing the boulder deposits to be stratigraphically correlated with the other evidence of overwash (Watt et al., this volume) and radiocarbon dating of the event (Atwater et al., this volume). Because the cobble and boulder fields are located in the flat interior of the island, issues related to the hydrodynamics of wave breaking on the reef crest and shoreline and the effect on boulder transport are avoided. The boulders are tabular in shape and composed of low-porosity limestone, well approximated by simple Cartesian methods (Spiske et al. 2008) of calculating volume and area. Through the use of high-resolution overwash simulations and detailed sensitivity analysis, we address the relative importance of the drag, inertia, and lift forces, uncertainty in semi-empirical coefficients, long-axis orientation, and overturning versus sliding transport mechanisms.

Anegada is the island closest to the North America Caribbean plate boundary north of Puerto Rico and the United States and British Virgin Islands (Fig. 1a). The northern Caribbean islands are impacted annually by hurricanes and have a poorly documented risk for transoceanic tsunamis (e.g. 1755 Lisbon tsunami and its predecessors) and local tsunamis (Atwater et al., this volume). Atwater et al. (this volume) outline geologic evidence for a catastrophic hurricane or tsunami, which inundated the northern coast and low lying

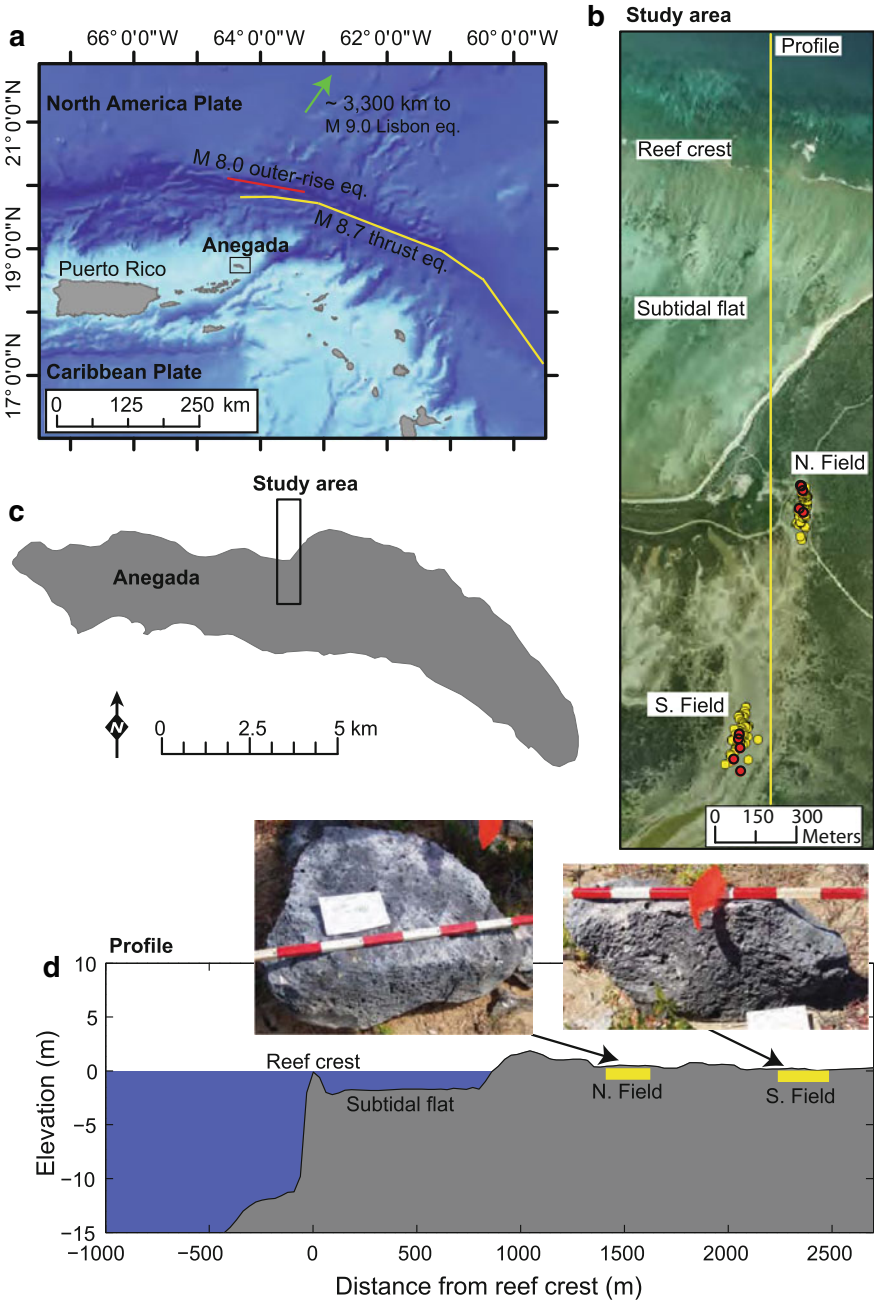


Fig. 1 Location map for Anegada (a), island map (c), aerial photograph of the study area (b), and topographic profile through the boulder fields (d). The rupture areas of the northern Antilles thrust earthquake of M 8.7 (yellow line) and the Puerto Rico Trench outer-rise earthquake of M 8.0 (red line) are given in Fig. 1a. The Lisbon earthquake of M 9.0 (green arrow) occurred ~ 3,300 km to the northeast off the coast of Portugal. Yellow symbols in Fig. 1b give the locations of all measured clasts; red symbols give the locations of the five largest boulders. The vertical yellow line in Fig. 1b is the location of the profile (Fig. 1d)

interior of Anegada sometime between 1650 and 1800. Evidence of overwash includes breaches through sandy beach ridges, a sheet of sand and shell capped with lime mud, and inland fields of cobbles and boulders (Atwater et al., this volume).

The overwash event identified by Atwater et al. (this volume) may have resulted from the transatlantic Lisbon tsunami of 1755, the Antilles tsunami of 1650, a local tsunami not previously documented, or a storm. In the 505 years from 1498 to 2002, there were 91 reported tsunamis in the Caribbean basin, of which 27 events are very well documented and caused extensive damage and casualties (Lander et al. 2002). In the 159 years from 1851 to 2009, a total of 60 tropical cyclone systems have been documented passing within 100 km of Anegada; 30 of these cyclones were tropical storms, eight category 1, 11 category 2, eight category 3, and three category 4, while no category 5 hurricane was reported (<http://csc-s-maps-q.csc.noaa.gov/hurricanes>; last accessed January 5, 2010). Here, we simulate overwash by the storm surge and storm waves of a category 5 hurricane and by tsunamis from a Lisbon earthquake of M 9.0 (Muir-Wood and Mignan 2009; Fig. 1a, green arrow), an earthquake of M 8.7 on a thrust fault in the northern Antilles subduction zone (Fig. 1a, yellow line), and an earthquake of M 8.0 on a normal fault on the outer rise along the Puerto Rico Trench (Fig. 1a, red line).

Boulders found in the interior of Anegada are used to estimate the minimum flow velocity that an overwash event must have generated in order to form the observed deposit. Estimates of the near-bed flow velocities required to transport the observed boulders are calculated using a simple inverse sediment-transport model, which accounts for fluid drag, inertia, buoyancy, and lift forces on boulders and includes both sliding and overturning transport mechanisms. Estimated near-bed flow velocities are converted to depth-averaged flow velocities using a linear eddy viscosity model and compared with water level and depth-averaged velocity time series from coastal inundation models. In this manner, potential causes for the overwash event on Anegada are evaluated.

1.1 Setting

Anegada (Fig. 1) extends 17 km along a west to southeast arc, covering 54 km² (Dunne and Brown 1979). It is flanked on its windward (north and northeast) side by a fringing coral reef (Fig. 1b). Between the reef and the north shore is a sandy subtidal flat extending 50 to 1,500 m from the shore (Figs. 1b and 1d). A carbonate sand beach rises into a series of beach ridges with maximum elevations 2 to 4 m above sea level (Watt et al., this volume). The interior of the island consists mostly of limestone, probably Pleistocene in age (Howard 1970; Horsfield 1975) that crops out mainly in the east and rises no more than 8 m above sea level. Shallow hypersaline salt ponds cover much of the western portion of the island.

1.2 Morphology of cobble and boulder fields

The cobble and boulder deposits form two isolated fields (referred to as North Field and South Field; Fig. 1b,d) along a relatively flat north–south trending topographic low (Fig. 1b,d). Based on field observations and clast lithology, Watt et al. (this volume) determined that the transported cobbles and boulders were derived from inland limestone outcrops. Transport distances range from several to 100's of meters (Watt et al., this volume). Measurements of clast location, axis lengths, long-axis orientation, depositional setting, and clast density are reported by Watt et al. (this volume). In total, 91 clasts were

measured ranging from 4 to 830 kg at the Northern Field, and 70 clasts were measured ranging from 1.5 to 414 kg at the Southern Field. Clasts measured were tabular in shape with an average shape factor, $CSF = C/\sqrt{AB}$ where A , B , and C are the primary axis lengths in descending order of length (Corey 1949) of 0.52 for the Northern Field and 0.41 for the Southern Field. Clasts were composed of low-porosity lithified limestone, with an average density of 2,400 kg/m³.

2 Methods

2.1 Coastal inundation models

2.1.1 Bathymetry and topography

Accurate bathymetric and topographic data are key inputs to accurate inundation modeling of storm or tsunami waves. Electronic Supplement 1 summarizes the density, resolution, datum, and sources of the bathymetric and topographic data used in the simulations. Differential GPS (DGPS) surveys conducted in 2009 by Watt et al. (this volume) provided extensive vertical control for the beach ridges and boulder fields.

2.1.2 Tsunamis

Tsunami simulations were performed with the Method of Splitting Tsunami (MOST) suite of numerical simulation codes, which is capable of simulating tsunami generation, trans-oceanic propagation, and inundation (Titov and Synolakis 1998). The MOST model has been extensively tested against a number of laboratory experiments and benchmarks (Synolakis et al. 2008) and was successfully used for simulations of many historical tsunami events (Titov et al. 2005; Wei et al. 2008; Titov 2009; Tang et al. 2009). Tsunamis from a Lisbon earthquake of M 9.0 (Fig. 1a, green arrow), an earthquake of M 8.7 on a thrust fault in the northern Antilles subduction zone (Fig. 1a, yellow line), and an earthquake of M 8.0 on a normal fault on the outer rise along the Puerto Rico Trench (Fig. 1a, red line) were simulated. Earthquake source parameters for these events are provided in Electronic Supplement 2. Simulations were performed in a depth-averaged 2-D mode with an output time step of 10 s (~60 samples per wavelength for a 10-min period tsunami) and a grid resolution of 30 m at the boulder fields. Bottom roughness was specified using a Manning's n of 0.03.

2.1.3 Storms

The hurricane simulation employs a Boussinesq-type numerical model (COULWAVE) for transformation of fully nonlinear and weakly dispersive waves in intermediate and shallow water (Lynett et al. 2002). Readers are referred to Lynett et al. (2002) for a thorough description and validation of this Boussinesq model. COULWAVE was used to simulate a category 5 hurricane with maximum sustained winds of 78 m/s, generating swells constructed using a JONSWAP spectrum (Hasselmann et al. 1973) with a dominant period of 17 s. Storm surge effects, resulting from barometric pressure, wind setup, and wave setup, were modeled as a uniform 1-m sea-level rise. The simulated hurricane exceeds the intensity of any storm impacting Anegada in the historical record (1851–2009;

<http://csc-s-maps-q.csc.noaa.gov/hurricanes>; last accessed January 5, 2010) and exceeds the 100-year return period wind speed (~ 55 m/s to 60 m/s), wave height (~ 7 m), and storm surge (~ 0.75 m) predicted for offshore the north coast of Anegada by the Caribbean Disaster Mitigation Project (CDMP; <http://www.oas.org/cdmp/document/reglstrm/index.htm>; last accessed January 5, 2010). Simulations were performed in a depth-averaged profile mode with a grid resolution of 10 m and an output time step of 0.12 s (~ 140 samples per wavelength for a 17-s period wave). The profile used in the simulation (Fig. 1d) is a north–south transect through the two boulder fields extracted from the 2D digital elevation model developed for the tsunami simulations. Bottom roughness was specified using a physical roughness, $z_o = 0.01$ m.

2.2 Sediment-transport model

Estimates of the near-bed flow velocities required to transport the observed boulders are calculated using a simple sediment-transport model, which accounts for fluid drag, inertia, buoyancy, and lift forces on boulders and includes both sliding and overturning transport mechanisms. Figure 2 is a diagram of the forces acting on a submerged boulder in an unsteady flow. The drag force (F_D) and inertia force (F_I) are estimated using the semi-empirical Morison equation (O’Brien and Morison 1952)

$$F_D = \frac{1}{2} C_D \rho_f A_{\perp} u^2 \tag{1}$$

$$F_I = C_M \rho_f V \dot{u} \tag{2}$$

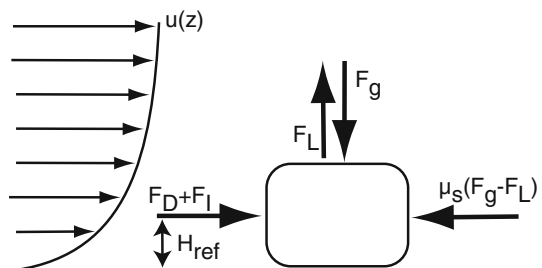
where C_D and C_M are the dimensionless coefficients of drag and inertia, respectively (See Sect. 2.3.1 for values), ρ_f is the fluid density (taken as $1,030 \text{ kg/m}^{-3}$), A_{\perp} is the cross-sectional area of the boulder normal to the flow, V is the boulder volume, u is the free stream flow velocity at a reference height above the bed (H_{ref}), and \dot{u} is the temporal flow acceleration ($\partial u / \partial t$). Following Helley (1969), H_{ref} is taken as $0.6 \times$ vertical-axis length (usually the C -axis). The velocity at H_{ref} is hereafter referred to as the near-bed velocity.

For flow in the vicinity of a boundary, a lift force acts on the particle (Einstein and El-Samni 1949). The formulation for the lift force (F_L) is similar to the drag force, but acts in the vertical

$$F_L = \frac{1}{2} C_L \rho_f A_L u^2 \tag{3}$$

where C_L is the dimensionless coefficient of lift (See Sect. 2.3.2 for values), and A_L is the horizontal cross-sectional area of the boulder.

Fig. 2 Diagram of forces acting on a submerged boulder in unsteady flow with a sliding resistance force



Sliding occurs when

$$F_D + F_I > \mu_s(F_g - F_L) \tag{4}$$

where μ_s is the coefficient of static friction, and F_g , the downward force from gravity is

$$F_g = (\rho_s - \rho_f)V_g \tag{5}$$

ρ_s is the particle density (2,400 kg/m³), and g is gravitational acceleration. The boulder fields have very low slopes allowing bed slope considerations to be neglected from the force formulations. Solving Eq. 4 for the minimum near-bed velocity for sliding (u_{slide}) gives

$$u_{slide} = \sqrt{\frac{\mu_s F_g - F_I}{0.5 \rho_f (C_D A_{\perp} + \mu_s C_L A_L)}} \tag{6}$$

For boulder overturning, the sum of the drag, inertia, and lift force moments must exceed the gravitational moment (Noormets et al. 2004)

$$F_D l_D + F_I l_I + F_L l_L > F_g l_g \tag{7}$$

where l_D , l_I , and l_L are the moment arms of the drag, inertia, and lift forces, and l_g is the gravitational moment arm. Solving Eq. 7 for the minimum near-bed velocity for boulder overturning, u_{over} .

$$u_{over} = \sqrt{\frac{l_g F_g - l_I F_I}{0.5 \rho_f (l_D C_D A_{\perp} + l_L C_L A_L)}} \tag{8}$$

Assuming the clast is pivoting on the axis parallel to flow at bed level, l_D and l_I are equal the height of the center of the drag force and inertia force, H_{ref} and l_L and l_g equal half the parallel axis length (Fig. 2).

To relate the calculated near-bed velocities to depth-averaged velocities, it is necessary to assume a vertical velocity profile. Here, a linear eddy viscosity model consistent with fully turbulent flow is implemented (Puleo et al. 2004).

$$u_* = \frac{U}{\frac{1}{\kappa H} \int_0^H \ln\left(\frac{z+z_0}{z_0}\right) dz} \tag{9}$$

where u_* is the friction velocity, U is depth-averaged velocity, κ is von Karman’s constant (0.41), H is water depth, z is elevation above the bed, and z_0 is the local roughness height. Velocity at layer k , u_k is

$$u_k = \frac{u_*}{k(z_{k-1} - z_k)} \int_{z_k}^{z_{k-1}} \ln\left(\frac{z+z_0}{z_0}\right) dz \tag{10}$$

Minimum velocities for sliding and overturning are calculated for the five largest boulders at the Northern and Southern Fields (Fig. 1b, red circles). The largest boulders are used to constrain the minimum flow velocity an event must generate to form the observed deposit. Fracturing of some boulders may have occurred during transport. If larger boulder were transported but not preserved in the deposit then the calculated minimum flow velocity is an underestimate. Average values for the largest boulders are used to simplify presentation of results and minimize the potential error from using a single clast (Table 1).

Table 1 Characteristics of the five largest boulders measured at the Northern and Southern Fields. The five largest boulders are used to calculate the minimum flow velocity of the overwash

	Northern Field		Southern Field	
	Mean	SD	Mean	SD
A-axis (m)	0.99	0.18	0.70	0.10
B-axis (m)	0.68	0.10	0.53	0.12
C-axis (m)	0.38	0.04	0.24	0.05
CSF	0.48	0.09	0.39	0.02
Volume (m ³)	0.26	0.06	0.09	0.05
Weight (kg)	625	154	228	125

2.3 Empirical coefficients and uncertainty

The sediment-transport model described above contains several empirical coefficients, which are poorly constrained for natural particle shapes in overwash type flow conditions. The approach taken here is to define a *general case* with coefficients chosen to be near the center of the value range published in the literature and perform sensitivity analysis to account for the full range of values published in the literature (see Sect. 3.2.1 for results). The choice of coefficient values and ranges are based on the particle shape and Reynolds number ($Re = uL/\nu$ where L is the particle length scale and ν is the kinematic viscosity) and is consistent with the previous studies. The coefficient values reported in the literature are outlined later. Table 2 lists the coefficients used in the *general case* and the coefficients that yield the maximum and minimum estimates of the minimum velocity for boulder transport. In order to solve for the minimum velocity for boulder transport, temporal flow acceleration must be known or assumed. In previous studies, temporal acceleration has been considered negligible (Goto et al. 2007; Goto et al. 2009), taken as a fixed value of 1 m/s^2 (Nott 2003), or calculated from a model-generated velocity time series (Goto et al. 2010). Here, we consider $\dot{u} = 0 \text{ m/s}^2$ and $\dot{u} = 1 \text{ m/s}^2$ (Table 2) and a range of temporal accelerations in the sensitivity analysis (see Sect. 3.1.2; Fig. 3), while using the calculated temporal accelerations from velocity time series for overwash simulations (Fig. 5).

2.3.1 Morison coefficients

Values of C_D in the literature for tabular boulders range from 1.05 (Imamura et al. 2008) to approximately 2 (Nott 2003; Goto et al. 2007; Noormets et al. 2004; Paris et al. 2009).

Table 2 Calculated near-bed flow velocities required to transport the largest boulders at the Northern and Southern Fields for the *general case* and for the coefficients which yield the maximum and minimum estimates of the minimum velocity for boulder transport. Results are given of steady flow and for a flow with a temporal acceleration of 1 m/s^2

Case	C_D	C_M	C_L	μ_s	Orientation	Northern Field		Southern Field	
						$\dot{u} = 0 \text{ m/s}^2$	$\dot{u} = 1 \text{ m/s}^2$	$\dot{u} = 0 \text{ m/s}^2$	$\dot{u} = 1 \text{ m/s}^2$
						$u_{\text{slide}} \text{ (m/s)}$	$u_{\text{slide}} \text{ (m/s)}$	$u_{\text{slide}} \text{ (m/s)}$	$u_{\text{slide}} \text{ (m/s)}$
<i>General</i>	1.5	2.0	0.178	0.6	Measured	2.6	2.3	2.3	2.1
<i>Minimum velocity</i>	2.0	2.5	0.4	0.4	Normal	1.8	1.3	1.5	1.1
<i>Maximum velocity</i>	1.0	1.5	0.1	0.8	Parallel	4.1	3.8	3.4	3.2

Values of C_M in the literature for tabular boulders range from 1.67 (Imamura et al. 2008) to 2 (Nott 2003). Here, we use $CD = 1.5$ and $CM = 2.0$ for the *general case* and $C_D = 1.5 \pm 0.5$ and $C_M = 2.0 \pm 0.5$ in the sensitivity analysis (see Sect. 3.1.2).

2.3.2 Lift coefficient

In experiments performed by Einstein and El-Samni (1949), C_L was calculated as 0.178 for a hemisphere fixed to the bed. Following Helley (1969) and Nott (2003), $C_L = 0.178$ is used for the *general case*. Cheng and Chiew (1998) suggested a lower bound of 0.1 and an upper bound of 0.4 for C_L , which are considered in the sensitivity analysis (see Sect. 3.1.2).

2.3.3 Friction coefficient

Studies of boulders transported on basalt (Noormets et al. 2004) and sand-covered limestone (Goto et al. 2007) platforms used $\mu_s \approx 0.7$. Voropayev et al. (2001) determined μ_s to be at between 0.5 and 0.8 in their laboratory studies with disk-shaped fiberglass cobbles on an immovable sand bed. In this study, irregular limestone boulders slide on a movable bed of sand or sand-covered limestone. $\mu_s = 0.6$ is used for the general case, and $\mu_s = 0.6 \pm 0.2$ is used in the sensitivity analysis (see Sect. 3.1.2).

3 Results

3.1 Minimum velocity for boulder transport

3.1.1 Overturning versus sliding

The calculated minimum near-bed velocities necessary to transport the largest boulders by sliding under steady flow are 2.6 m/s at the Northern Field and 2.3 m/s at the Southern Field (Table 2, *general case*; $\dot{u} = 0 \text{ m/s}^2$). Minimum velocities required to overturn the boulders are higher, with near-bed velocities of 3.9 m/s for the Northern Field and 3.6 m/s for the Southern Field. From Eqs. 4 and 7, for the velocities necessary to slide boulders to be greater than those needed to overturn boulders, μ_s must be greater than $\frac{5}{6} \frac{\parallel \text{axis}}{\uparrow \text{axis}}$, where \parallel axis is the parallel axis length, and \uparrow axis is the vertical-axis length.

The \parallel axis is nearly always greater than or equal to \uparrow axis because boulders tend to be positioned with their shortest axis vertical. Taking \parallel axis = \uparrow axis, the minimum possible μ_s for overturning to occur at a lower velocity than required for sliding would be 0.833. This value is greater than the maximum μ_s considered here. Given that sliding occurs at lower flow velocities than overturning and the lack of field evidence for overturning, sliding is assumed as the transport mechanism when calculating the minimum velocities for boulder transport.

3.1.2 Sensitivity analysis

Using the coefficients that yield the maximum and minimum estimates gives a range of minimum near-bed velocities for the transport of the largest boulders at the Northern Field from 1.8 m/s to 4.1 m/s and at the Southern Field from 1.5 m/s to 3.4 m/s (Table 2, minimum and maximum velocity bounds with $\dot{u} = 0 \text{ m/s}^2$). Uncertainties resulting from

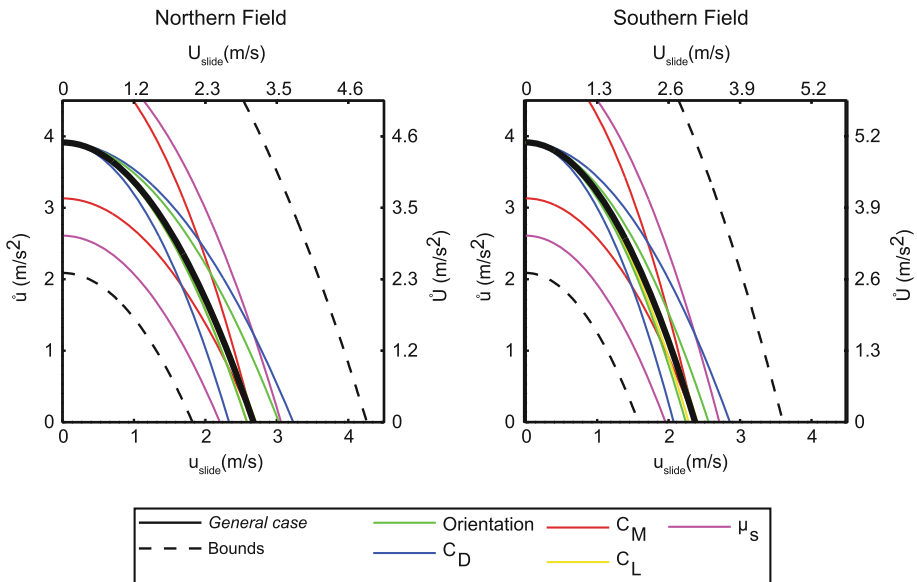


Fig. 3 Curves give estimates of minimum velocity and temporal acceleration required for transport of the average of the five largest boulders at the Northern (first column) and Southern Fields (second column) for a range of coefficients. The primary axes give the near-bed velocity (u_{slide}) and temporal acceleration (\dot{u}), and the secondary axes give the corresponding depth-averaged velocity (U_{slide}) and temporal acceleration (\dot{U}) assuming a linear eddy viscosity profile with $z_o = 0.01$ m and a flow depth of 1 m (approximate flow depth at boulder fields from simulations). The solid black curve gives the *general case*; *dashed curves* give the maximum and minimum estimates of the minimum velocity for boulder transport (see Table 2 for values used). *Colored lines* show the effect of varying coefficients individually while keeping other parameters the same as the *general case* (see Table 2)

variation in temporal acceleration, particle orientation, drag coefficient, inertia coefficient, lift coefficient, and static friction coefficient are considered in Fig. 3. The friction coefficient is the largest source of uncertainty, accounting for approximately half of the total uncertainty (Fig. 3, magenta lines). Results are sensitive to changes in the drag coefficient and long-axis orientation (Fig. 3, blue and green curves, respectively) at low temporal accelerations, but the choice of the inertia coefficient (Fig. 3, red curves) becomes increasingly important at temporal accelerations greater than approximately 2.5 m/s^2 . If temporal acceleration is unknown, $\dot{u} = 1 \text{ m/s}^2 \pm 1$ introduces an uncertainty in the calculated near-bed velocity roughly equivalent to the uncertainty introduced by drag coefficient under steady flow.

3.2 Overwash simulations

The simulated hurricane and tsunamis have distinct landward maximum water level and velocity decay profiles (Figs. 4a and 4b, respectively). Shoaling at the reef crest is most pronounced for a simulated category 5 hurricane (Fig. 4a, black curve) and a tsunami from a M 8.0 Puerto Rico Trench outer-rise earthquake (Fig. 4a, red curve). Water levels and velocities decay strongly over the subtidal flat for a category 5 hurricane; onshore the maximum water levels remains relatively constant whereas the velocities decrease further.

Tsunamis from a Lisbon earthquake of M 9.0 and a northern Antilles subduction zone thrust earthquake of M 8.7 have similar onshore water level and velocity decay trends. In these two simulations, the maximum water levels remain relatively constant over the profile, while the velocities increase over the topographic highs of the reef crest and shoreline (Fig. 4, green and magenta curves).

Over the 1.4 km from the reef crest to the Northern Field, the maximum water level decreases by 48%, 43%, and 73% and the maximum velocities decreases by 58%, 52%, and 54% for tsunamis from a Lisbon M 9.0, a northern Antilles thrust M 8.7, and a Puerto Rico Trench outer-rise M 8.0 earthquakes, respectively. The maximum water level for a category 5 hurricane decreases by 75%, and the maximum velocity decreases by 85%. The Froude number ($F_r = U/\sqrt{gH}$ where U is the flow speed, g is acceleration due to gravity, and H is flow depth) is a nondimensional number that describes whether a flow is supercritical (>1), critical (=1) or subcritical (<1). Froude numbers at the time of the maximum velocity at the Northern Field are 0.64, 0.84, and 0.90 for tsunamis from a Lisbon M 9.0, a northern Antilles thrust M 8.7, and a Puerto Rico Trench outer-rise M 8.0 earthquakes, respectively. The corresponding Froude number for the category 5 hurricane is 0.32.

Over the 835 m from the North Field to the South Field, the maximum water level decreases by 1.4, 35, and 20% and the maximum velocities decreases by 12, 34, and 25% for tsunamis from a Lisbon M 9.0, a northern Antilles thrust M 8.7, and a Puerto Rico Trench outer-rise M 8.0 earthquakes, respectively. The maximum water level for a category 5 hurricane increases by 8%, while the velocity decreases by 48%. Froude numbers at the time of the maximum velocity at the Southern Field are 0.61, 0.66, and 0.87 for

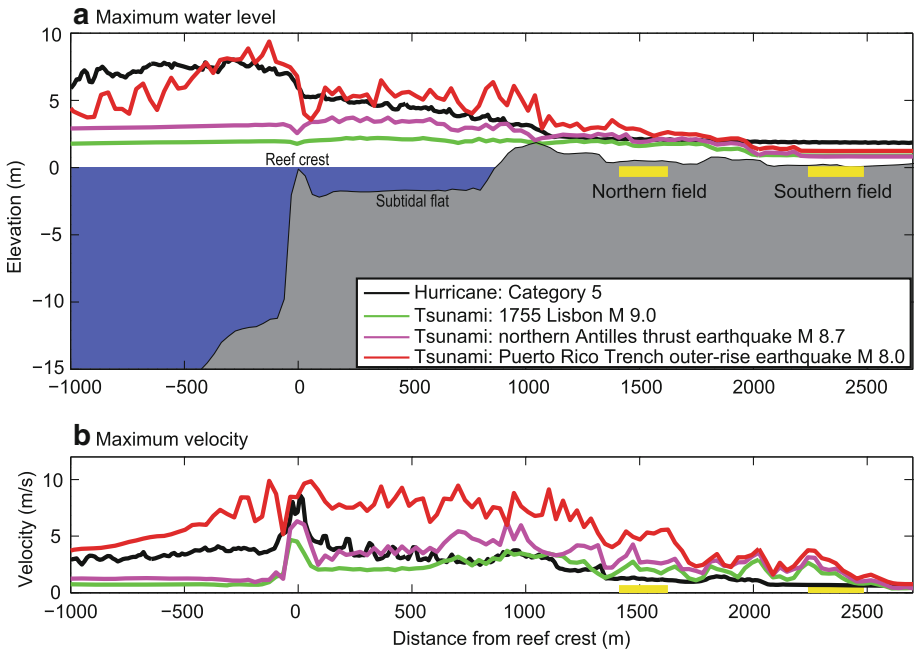


Fig. 4 Maximum water levels and depth-averaged velocities along a profile (Fig. 1b, yellow line) across Aneгада’s fringing reef, the tidal flat behind it, and the onshore areas that include the Northern and Southern Fields

tsunamis from a Lisbon M 9.0, a northern Antilles thrust M 8.7, and a Puerto Rico Trench outer-rise M 8.0 earthquakes, respectively. The corresponding Froude number for a category 5 hurricane is 0.14.

Figure 5 shows time series of water level (blue lines) and velocity (red lines) in 25-m water depth at a location 1 km offshore of the reef crest and at the center of the two boulder fields. The offshore waveforms of the simulated tsunamis (Fig. 5 top row) vary in orientation of the leading wave, number of waves, and period of the waves. A category 5 hurricane generates waves with larger offshore amplitudes (approximately 10 m) than any of the simulated tsunamis, but much shorter periods (dominant period of 17 s). At the Northern Field (Fig. 5, middle row), the tsunami from a Lisbon earthquake of M 9.0 strikes with a series of waves of approximately the same amplitude. Tsunamis from a M 8.7 and a M 8.0 near-field earthquakes have a single large leading wave followed by smaller ones. Wave fronts from a category 5 hurricane arrive at the Northern Field at approximately a 3.5-min interval. The water level gradually increases with successive wave fronts filling the topographic low. At the Southern Field (Fig. 5, bottom row), the tsunamis arrive as a

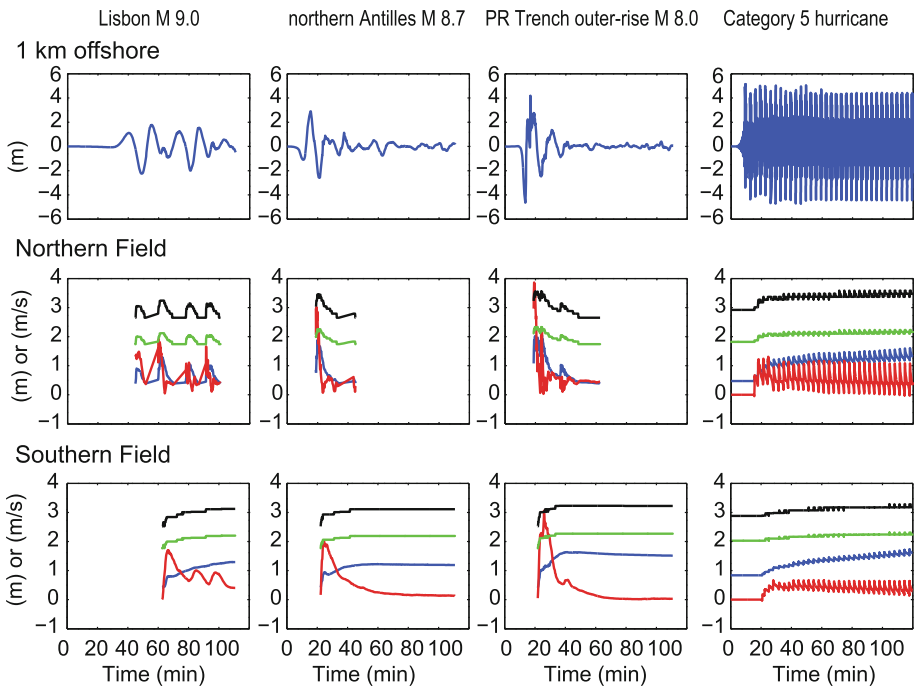


Fig. 5 Time series of water level (blue line) and depth-averaged velocity (red line) at three locations: 1 km offshore of the reef crest in 25-m water depth (top row), the center of the Northern Field (middle row), and the center of the Southern Field (bottom row). Velocity time series from four simulated overwash events are compared with the minimum depth-averaged velocity estimates for transport of the average of the five largest boulders at the two fields, assuming the general case (black curve) and the set of coefficients that yield the lowest necessary velocities (green curve). Boulder transport occurs when the modeled velocity (red curve) exceeds the estimated minimum velocity (black curve for the general case or green curve for the set of coefficients, which yield the lowest necessary velocities). 6.6 h have been subtracted from the time scale for a Lisbon earthquake to allow for propagation across the Atlantic. Portions of the time series where flow depths are not great enough to fully submerge the largest boulders have been removed

single water level surge. The water level time series for a category 5 hurricane is similar to the time series at the Northern Field, but with a decrease in the amplitude of wave fronts.

The maximum temporal acceleration calculated for a category 5 hurricane is 0.18 m/s^2 at the Northern Field and 0.07 m/s^2 at the Southern Field. The maximum \dot{u} calculated for the simulated tsunamis is 0.19 m/s^2 at the Northern Field and 0.04 m/s^2 at the Southern Field.

3.3 Predicted boulder transport

For the *general case*, a simulated Puerto Rico Trench outer-rise earthquake of M 8.0 is the only event that generates flow velocities necessary to transport the largest boulders at both inland boulder fields (*general case*; Fig. 5 column 3, red and black curves). A northern Antilles thrust earthquake of M 8.7 generates velocities high enough to transport the largest boulders at the Northern Field, but not the Southern Field. When using coefficients that result in the lowest estimates of the necessary velocities for boulder transport (Sect. 2.3 and 3.1.2), a tsunami generated by a northern Antilles thrust earthquake of M 8.7 is capable of transporting the largest boulders at both fields (Fig. 5, red and green curves). Therefore, it is possible that such an event may be capable of forming the observed boulder deposits. The tsunami from a Lisbon earthquake of M 9.0 and a category 5 hurricane inundate both fields, but generate depth-averaged velocities below the minimum value for transport of the largest boulders at both fields. Even when using coefficients that yield the lowest estimates of the necessary velocities for boulder transport (Sect. 2.3 and 3.1.2), a tsunami from a Lisbon earthquake of M 9.0 and a category 5 hurricane can be excluded from transporting the largest boulders at the two boulder fields (Fig. 5, red and green curves).

4 Discussion

A large-clast sediment-transport model was used to estimate the minimum flow velocity of overwash generated by a tsunami or a storm striking Anegada, BVI a few centuries ago. The calculated minimum near-bed velocities necessary to slide the largest boulders under steady flow are 2.6 m/s at the Northern Field and 2.3 m/s at the Southern Field (Table 2, *general case*, $\dot{u} = 0 \text{ m/s}^2$). It is found that μ_s must be greater than $\frac{5}{6} \frac{||\text{axis}}{|\text{axis}|}$ for overturning to occur at a lower velocity than sliding (see Sect. 3.1.1); this relationship yields μ_s values greater than those found in the literature. This does not mean that overturning of boulders has not occurred, but without field evidence suggesting a transport mechanism, the transport mechanism that predicts the lowest required velocity must be assumed.

Empirical coefficients used in the large-clast sediment-transport model were estimated from laboratory experiments performed in previous studies, but are poorly constrained for natural particles in overwash flows. To estimate the uncertainty, in Sect. 3.1 we varied the empirical coefficients used in the drag, inertia, lift, and resistance force calculations based on ranges found in the literature for blocky boulders in high Reynolds number flows. For steady flow, the estimates of minimum velocity for boulder transport ranged from 1.8 m/s to 4.1 m/s at Northern Field and 1.5 m/s to 3.4 m/s for the Southern Field, approximately a factor of two changes. Morton et al. (2006) address the importance of the inertia force in the overall force balance. In Sect. 3.1.2, the inertia force is shown to be small relative to the drag force for temporal accelerations below approximately 1 m/s^2 .

To determine which events are capable of transporting the observed boulders, we compared the estimates of the flow velocity required to transport the largest boulders to time series from simulated storms and tsunamis. The numerical simulations model the propagation, shoaling, and overwash for waves of a category 5 hurricane and for three tsunamis. Despite having maximum flow depths greater than the tsunamis, a category 5 hurricane generated comparatively low flow velocities. Froude numbers at the time of maximum flow velocities at the two fields range from 0.6 to 0.9 for the tsunamis; Froude numbers at the time of the maximum flow velocity for a category 5 hurricane are much lower, 0.3 at Northern Field and 0.1 at the Southern Field.

Velocity decay landward of the reef crest is found to be the determining factor in assessing boulder transport at the inland boulder fields. At the reef crest, all of the simulated events generate velocities high enough to transport the largest boulders observed at Anegada. Velocities decay toward the boulder fields as wave energy dissipates due to wave breaking and bottom friction over the reef crest, subtidal flat, and beach ridges. The magnitude of velocity decay is much greater for the shorter period storm waves than the long period tsunami waves. Results show that despite generating high velocities over the reef crest and subtidal flat and inundating the boulder fields, the rapid dissipation of storm waves from a category 5 hurricane prevents transport of the largest boulders at the two inland boulder fields.

In addition to the high velocities generated by the simulated events at the reef crest, subtidal flat, and shoreline, calculated temporal accelerations are also high at these locations. Maximum temporal accelerations decrease with distance inland to a maximum calculated value of 0.19 m/s^2 for all events at the boulder fields. It should be noted that actual temporal accelerations maybe greater than the calculated maximum value at the passage of wave crests because of limitations in the hydrodynamic models and the output time steps used. A temporal acceleration of 0.19 m/s^2 yields a negligible inertia force in the overall force balance for boulder transport. The dominant fluid force under these conditions is the drag force that is proportional to the flow velocity squared. The velocity and temporal acceleration are out of phase, when drag force is the greatest the inertia force is zero. This phase relationship further reduces the importance of the inertia force.

All of the simulated overwash events are shown to be capable of transporting large boulders near the reef crest; however, wave energy attenuation limits the size of boulders that can be moved at the two boulder fields in the interior of Anegada. Only a tsunami generated by a simulated near-field Puerto Rico Trench outer-rise earthquake of M 8.0 generates velocities necessary to transport (using the *general case* coefficients) the largest boulders at the two cobble and boulder fields. The tsunami from a Lisbon earthquake of M 9.0, the tsunami from a thrust earthquake of M 8.7 on the northern Antilles subduction zone, and the storm surge and waves from a category 5 hurricane inundated the two fields but did not generate velocities sufficient to transport the largest boulders (using the *general case* coefficients). Even when considering the uncertainty introduced by the empirical coefficients (Sect. 3.3), a Lisbon earthquake of M 9.0 and a category 5 hurricane are not capable of transporting the largest boulders.

The numerical simulations allow for assessment of inundation trends but do not allow for detailed analysis of small-scale flow modifications by topographic features including reef channels, thalwegs, and knolls that are likely important to water level and velocity time series at specific points in the cobble and boulder fields. The 30-m grid resolution used on land in the tsunami simulations limits the scale of features that can be resolved, and the profile modeling of a hurricane does not include any alongshore variation. In order to further constrain the source event, additional higher resolution modeling needs to be performed including 2-D

horizontal hurricane simulations. The collection of additional nearshore and onshore elevation data would greatly improve the resolution and accuracy obtainable in future modeling studies. With higher resolution simulations, it will be possible to perform 2-D horizontal cobble and boulder transport modeling, allowing not only for a refined comparison of modeled and calculated velocities, but also the ability to model the spatial distribution of transported clasts that can be compared to observed clast distributions.

5 Conclusions

Linking forward hydrodynamic models with a large-clast inverse sediment-transport model allows for a quantitative determination of the capacity of a storm or tsunami to produce overwash capable of emplacing inland fields of boulders at Anegada, British Virgin Islands. Despite limitations in the boulder transport formulations and the numerical modeling, it appears unlikely that waves generated by a category 5 hurricane can sustain velocities high enough to transport the largest boulders observed in the interior of Anegada. Simulated storm surge and waves of a category 5 hurricane and tsunamis from a Lisbon earthquake of M 9.0 and two hypothetical earthquakes along the North America Caribbean Plate boundary generate high flow velocities and temporal acceleration at the reef crest, subtidal flat, and shoreline capable of moving the largest observed boulders, but wave energy attenuation limits the size of boulders able to be transported at the inland boulder fields. Of the simulated events, the tsunami generated by an earthquake of M 8.0 on a normal fault of the outer rise along the Puerto Rico Trench is the most capable of transporting the observed cobbles and boulders on Anegada.

Acknowledgments This work was carried out as part of the US Geological Survey's "Tsunami Hazards Potential in the Caribbean" project. We would like to thank Brian Atwater, Uri ten Brink, Alex Apotsos and Jeff Hansen for their numerous excellent suggestions to improve the manuscript and a timely review of our work. We would also like to thank the two anonymous referees who provided detailed comments and suggestions that also improved the manuscript.

References

- Atwater BF, ten Brink US, Buckley M, Halley RS, Jaffe BE, Lopez Venagas AM, Reinhardt EG, Tuttle MP, Watt S, Wei Y (this volume) Geomorphic and stratigraphic evidence for an unusual tsunami or storm a few centuries ago at Anegada, British Virgin Islands. *Natural Hazards*
- Caribbean Disaster Mitigation Project (2002) Atlas of probable storm effects in the Caribbean Sea. <http://www.oas.org/CDMP/document/reglstrm/Hurratlas7D.ppt>
- Cheng NS, Chiew YM (1998) Pick-up probability for sediment entrainment. *J Hydraul Eng ASCE* 124(2):232–235
- Corey AT (1949) Influence of shape on fall velocity of sand grains. Unpublished Msc thesis, Colorado A&M College, p 102
- Dawson AG, Stewart I, Morton RA, Richmond BM, Jaffe BE, Gelfenbaum G (2008) Reply to Comments by Kelletat (2008) comments to Dawson, A.G. and Stewart, I. (2007) Tsunami deposits in the geological record [*Sedimentary Geology*, 200, 166–183]. *Sediment Geol* 211:92–93
- Dunne RP, Brown BE (1979) Some aspects of the ecology of reefs surrounding Anegada, British Virgin Islands. Atoll research bulletin 236. The Smithsonian Institution, Washington, DC
- Einstein HA, El-Samni EA (1949) Hydrodynamic forces on a rough wall. *Rev Modern Phys* 21:520–524
- Goff J, Dudley WC, deMaintenon MJ, Cain G, Coney JP (2006) The largest local tsunami in 20th century Hawaii. *Mar Geol* 226:65–79

- Goto K, Chavanich SA, Imamura F, Kunthasap P, Matsui T, Minoura K, Sugawara D, Yanagisawa H (2007) Distribution, origin and transport process of boulders deposited by the 2004 Indian Ocean tsunami at Pakarang Cape. *Thailand Sediment Geol* 202:821–837
- Goto K, Okada K, Imamura F (2009) Characteristics and hydrodynamics of boulders transported by storm waves at Kudaka Island. *Jpn Mar Geol* 262:14–24
- Goto K, Okada K, Imamura F (2010) Numerical analysis of boulder transport by the 2004 Indian Ocean tsunami at Pakarang Cape. *Thailand Mar Geol* 268:97–105
- Hall AM, Hansom JD, Williams DM, Jarvis J (2006) Distribution, geomorphology and lithofacies of cliff-top storm deposits: examples from the high-energy coasts of Scotland and Ireland. *Mar Geol* 232: 131–155
- Hasselmann K, Barnett TP, Bouws E, Carlson H, Cartwright DE, Enke K, Ewing JA, Gienapp H, Hasselmann DE, Kruseman P, Meerburg A, Miller P, Olbers DJ, Richter K, Sell W, Walden H (1973) Measurements of wind-wave growth and swell decay during the Joint North Sea Wave Project (JONSWAP)'. *Ergänzungsheft zur Deutschen Hydrographischen Zeitschrift Reihe, A(8) (Nr. 12)*, 95
- Helley EJ (1969) Field measurement of the initiation of large bed particle motion in blue creek near Klamath, California. U.S. Geological Survey Professional Paper 562-G, 19 pp
- Horsfield WT (1975) Quaternary vertical movements in the Greater Antilles. *Geol Soc Am Bull* 86:933–938
- Howard J (1970) Reconnaissance geology of Anegada Island. Caribbean Research Institute, St. Thomas
- Imamura F, Goto K, Ohkubo S (2008) A numerical model for the transport of a boulder by tsunami. *J Geophys Res Ocean* 113:C01008. doi:10.1029/2007JC004170
- Lander JF, Whiteside LS, Lockridge PA (2002) A brief history of tsunami in the Caribbean Sea. *Sci Tsunami Hazards* 20(2):57–94
- Lynett PJ, Wu TR, Liu PL (2002) Modeling wave runup with depth-integrated equations. *Coast Eng* 46: 89–107
- Morton RA, Richmond BM, Jaffe BE, Gelfenbaum G (2006) Reconnaissance investigation of Caribbean extreme-wave deposits—Preliminary observations, interpretations, and research directions, US Geological Survey Open-File Report OFR-2006-1293, 42 pp. <http://pubs.usgs.gov/of/2006/1293/>
- Morton RA, Richmond BM, Jaffe BE, Gelfenbaum G (2008) Coarse clast coastal ridges of the Caribbean region: a reevaluation of processes and origins. *J Sediment Res* 78:624–637
- Muir-Wood R, Mignan A (2009) A phenomenological reconstruction of the Mw9 November 1st 1755 earthquake source. *The 1755 Lisbon Earthq* 7(Part III):121–146. doi:10.1007/978-1-4020-8609-0_8
- Noormets R, Crook KAW, Felton EA (2004) Sedimentology of rocky shorelines: 3: hydrodynamics of megaclast emplacement and transport on a shore platform, Oahu, Hawaii. *Sediment Geol* 172:41–65
- Nott J (2003) Waves, coastal boulder deposits and the importance of the pre-transport setting. *Earth Planet Sci Lett* 210:269–276
- O'Brien MP, Morison JR (1952) The forces exerted by waves on objects. *Trans Am Geophys Union* 33(1):32–38
- Paris R, Wassmer P, Sartohadi J, Lavigne F, Barthomeuf B, Desgages E, Grancher D, Baumert P, Vautier F, Brunstein D, Gomez C (2009) Tsunamis as geomorphic crises: lessons from the December 26, 2004 tsunami in Lhok Nga, West Banda Aceh (Sumatra, Indonesia). *Geomorphology* 104:59–72
- Puleo J, Mouraenko O, Hanes D (2004) One-dimensional wave bottom boundary layer model comparison: specific Eddy viscosity and turbulence closure models. *J Waterw Port Coast Ocean Eng* 130(6):322–325
- Spiske M, Böröcz Z, Bahlburg H (2008) The role of porosity in discriminating between tsunami and hurricane emplacement of boulders—a case study from the Lesser Antilles, southern Caribbean. *Earth Planet Sci Lett* 268:384–396
- Synolakis CE, Bernard EN, Titov VV, Kanaglu U, Gonzalez EI (2008) Validation and verification of tsunami numerical models. *Pure Appl Geophys* 165(11–12):2197–2228
- Tang L, Titov VV, Chamberlin CD (2009) Development, testing, and applications of site-specific tsunami inundation models for real-time forecasting. *J Geophys Res* 114:C12025. doi:10.1029/2009JC005476
- Titov VV (2009) Tsunami forecasting. Chapter 12 in *The Sea*, volume 15: Tsunamis. Harvard University Press, Cambridge, p 371
- Titov VV, Synolakis CE (1998) Numerical modeling of subtidal wave runup. *J Waterw Port Coast Ocean Eng* 124(4):157–171
- Titov VV, González FI, Bernard EN, Eble MC, Mofjeld HO, Newman JC, Venturato AJ (2005) Real-time tsunami forecasting: challenges and solutions. *Nat Hazards* 35(1):41–58 (Special Issue, U.S. National Tsunami Hazard Mitigation Program)
- Voropayev SI, Cense A, McEachern GB, Boyer DL, Fernando HJS (2001) Dynamics of cobbles in the shoaling region of a surf zone. *Ocean Eng* 28(7):763–788

- Wei Y, Bernard E, Tang L, Weiss R, Titov V, Moore C, Spillane M, Hopkins M, Kânođlu U (2008) Real-time experimental forecast of the Peruvian tsunami of August 2007 for US coastlines. *Geophys Res Lett* 35:L04609. doi:[10.1029/2007GL032250](https://doi.org/10.1029/2007GL032250)
- Watt S, Buckley M, Jaffe B (this volume) Inland fields of dispersed cobbles and boulders as evidence for a tsunami on Anegada, British Virgin Islands. *Nat Hazards*